# Effects of $NH_3$ and $N_2$ source gases and plasma excitation frequencies on the reaction chemistry for $Si_3N_4$ thin-film growth by remote plasma-enhanced chemical-vapor deposition

J. A. Theil, S. V. Hattangady, and G. Lucovsky
*Departments of Physics, and Materials Sciences and Engineering, North Carolina State University, Raleigh, North Carolina 27695-8202*

(Received 16 December 1991; accepted 16 March 1992)

$NH_3$/He and $N_2$/He discharges can produce qualitatively different silicon nitride films when they are used as N-atom sources in the remote plasma-enhanced chemical-vapor deposition process. Radio frequency and microwave excitation at frequencies, 13.56 MHz and 2.54 GHz, respectively, were used to produce significantly different electron temperatures $T_e$, electron energy distribution functions, and electron densities $n_e$. Differences in these plasma parameters were then correlated with important aspects of the silicon nitride reaction chemistry, including the incorporation of hydrogen in SiH and/or Si–NH bonding arrangements.

## I. INTRODUCTION

Today, there is a major thrust in the microelectronics industry toward process integration through the use of cluster tooling, and single chamber processing, including etching, and film deposition and growth. This type of integration frequently requires processes with low thermal budgets, including low-temperature plasma-enhanced chemical-vapor deposition (PECVD). The deposition of PECVD silicon nitrides is receiving interest for passivation and isolation layers, and also for constituent layers in (i) gate dielectrics for ultralarge scale integration (ULSI) devices, and (ii) oxide–nitride–oxide (ONO) dielectrics for storage capacitors in dynamic random access memory (DRAM) circuits. There has been a great deal of work in the area of silicon nitride thin-film deposition by PECVD.[1–7] Smith has shown in a radio frequency (rf) plasma-excited $SiH_4/N_2$ deposition atmosphere, that there are no homogeneously generated deposition precursors formed with Si–N bonds.[1] However, for an rf-excited $SiH_4/NH_3$ deposition atmosphere, aminosilane ($SiN_xH_y$, $x = 1$–4) ions are detected at high $NH_3$:$SiH_4$ ratios, and are believed to contribute as precursor species in heterogeneous thin-film deposition reactions.

The remote PECVD process affords greater control over the thin-film chemistry than the conventional PECVD processes by restricting plasma excitation to a subset of the process gases, and thereby reducing the number of possible reaction pathways. The physical arrangement of a remote PECVD chamber is designed to make the process flow *sequential or serial*, rather than *parallel* as in conventional direct PECVD processes such as those used by Smith.[1] The excited species extracted from the plasma excitation region of a remotely excited plasma reactor, and unexcited species injected downstream, generally react heterogeneously at the substrate to produce the desired thin film; however, homogeneous reactions may be involved in the formation of deposition reaction precursor species. For the deposition of $SiO_2$, $Si_3N_4$, and $SiO_xN_y$ alloys, the Si-atom source gases, such as $SiH_4$ and $Si_2H_6$, are always injected downstream, and are never directly exposed to the plasma in order to prevent gas-phase decomposition, and thereby restrict the number of silane fragments that can act as deposition precursors.

This paper studies the effects of different gas phase precursors on the deposition and composition of silicon nitride films. We specifically consider the effects of (i) different N-atom source gases: $N_2$ and $NH_3$, and (ii) plasma excitation at different frequencies: rf and microwave. There is considerable interest in the use of microwave, as well as radio frequency excitation for remote plasma reactors, and direct comparisons are needed to explain any significant differences in precursor formation, reaction pathways, and film properties that derive from excitation in different frequency regimes: in our study these are 13.56 MHz and 2.54 GHz. The remote PECVD process permits a study of the deposition process chemistry in ways that are not possible using conventional PECVD, simply because of chamber geometry and chamber fixturing. For example, it is relatively easy to change the powered electrode configuration so that studies of different power coupling methods may be made with the same chamber geometry for process gas injection and substrate placement. For example, one of the approaches employed in determining how different source gases and frequencies of plasma excitation influence deposition reactions and film properties will be to study deposition rates and film properties as a function of position of the substrate relative to both the plasma tube, and the down stream shower head injectors.

## II. EXPERIMENTAL APPROACH

### A. Chamber design

The deposition chamber used in this study has features that permit *in situ* analysis of the gas species in the chamber, and nonintrusive analysis of radiating species, at the same time a film is being deposited; however, we have not used the optical analysis capability in this study. The chamber has a 14.9 cm i.d., and is 56 cm in length (see Fig. 1). A 3.2-mm-diam fused silica tube is located at one end of the chamber, and is centered on the chamber axis. A

 0734-2101/92/040719-09$01.00 ©1992 American Vacuum Society 

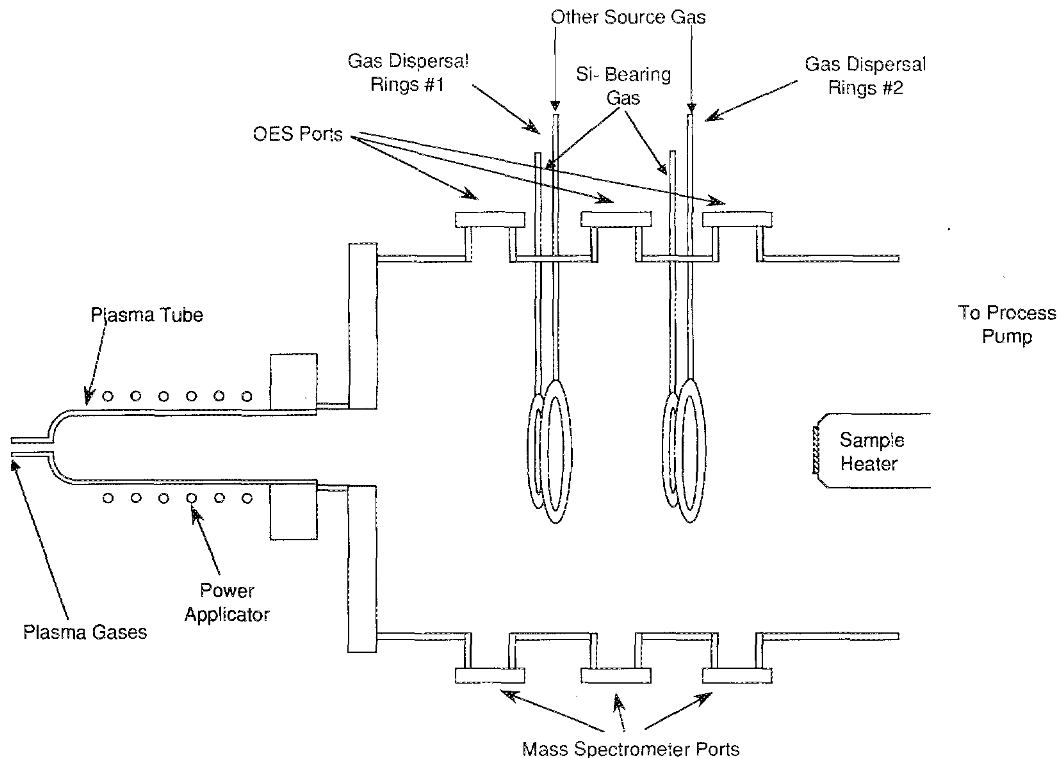


FIG. 1. Schematic of remote PECVD deposition chamber, showing diagnostic ports for optical emission spectroscopy (OES) and mass spectrometry.

ten-turn copper coil is used to couple 13.56 MHz rf power into the plasma, and a section of wave-guide is placed over the tube to couple microwave power at 2.54 GHz. A 400 ℓ/s turbomolecular pump is used to establish a base pressure of $\sim 5\times 10^{-8}$ Torr. There is a loadlock assembly at the opposite end of the chamber that accommodates an electrically floating piston-driven substrate holder/heater assembly. Inside the chamber, at 10.2 and 35.6 cm from the plasma tube flange, there are two sets of double showerhead gas dispersal rings for downstream injection of process gases. There are sampling stations located along the chamber in three locations: one midway between the plasma tube flange and the first set of dispersal rings, and two others, 3.8 cm downstream from each set of dispersal rings. Each station consists of two horizontal ports with pyrex windows for optical studies, and a vertical port to accommodate the sniffer tube of the mass spectrometer. The mass spectrometer has a 1.6-cm-diam sniffer tube that may be positioned in the chamber as much as 2.8 cm from the chamber wall. This tube is connected to an isolation gate valve assembly that opens into the mass spectrometer chamber, which can be pumped to base pressure of $< 10^9$ Torr.

## B. Plasma power coupling

The rf power applicator consists of a ten-turn copper coil that is wrapped around the plasma tube, and rf power is delivered from an rf generator through a coaxial cable via a matching network. The microwave power applicator is an ASTEX S-250 power supply, capable of generating a 0–250 W at 2.54 GHz, and is connected to a waveguide terminator with the plasma tube passing through the terminator at a position that maximizes coupling of the electric field to the plasma. Standard microwave components are used to monitor and tune the power coupling into the plasma. With this apparatus, it is relatively easy to ignite and maintain rf plasmas at power levels between 10 and 100 W, whereas microwave plasmas can only be maintained for power levels in excess of about 150 W.

## C. Instrumentation

The *in situ* instrumentation used in this study are the mass spectrometer and the Langmuir probe. The mass spectrometer is an EXTREL C-50 quadrupole unit with 3/8-in.-diam pole pieces. It is controlled by an IBM-AT computer using ASYST-based software. The mass spectrometer is connected to the remote PECVD chamber by a sniffer tube that, as noted above, protrudes into that chamber to within 4.3 cm of the chamber axis, or 2.8 cm from the chamber wall. Taking advantage of the 9 cm sniffer tube length, it is possible to filter out ions generated in the chamber and to then examine only neutral species, by simply placing a ceramic magnet against the length of the sniffer tube. Conversely, it is possible to examine only the plasma generated ions by removing the magnet, and turning off the ionizer in the mass spectrometer.

The Langmuir probe can be used to determine $n_e$ and $T_e$ of the plasma afterglow, where $n_e$ is the electron concentration, and $T_e$ is a measure of the average electron temperature. The Langmuir probe consists of a 0.95-cm-diam

Pyrex tube, approximately 10 cm long, with two platinum wire electrodes encased in 1 mm Pyrex sheaths, using a uranium-doped glass as the sealing bead. The probes protrude from the end of the tube with a spacing of 7 mm. The probe was mounted on the base-plate of the sample heater, so that the probe tips could be positioned anywhere along the axis of the chamber from just inside the plasma tube to the loadlock.

The double Langmuir probe utilizes two conductors so that a complete current path may be obtained independent of the ground, *minimizing* the disturbance of the plasma by the probes. In plasma afterglow regions, minimal disturbance is important, because the charge density is too low to make up for any charge collected by the probes. The double-probe current-voltage characteristic is similar to the single probe curve, but the magnitude of the respective saturation curves is a function of the probe areas so that keeping these areas the same simplifies data reduction. The logarithmic plot method of Johnson and Malter was used to calculate the $T_e$, because it is not sensitive to offset currents at small voltages.[8] Once $T_e$ is determined it is possible to calculate the ion and electron densities. The charged density equation comes from the approximation of Bohm, Burhop, and Massey that uses a constant voltage approximation for the saturation ion flux.[9] The approximation assumes a constant sheath area which gives an order of magnitude estimate by

$$I_0=\frac{1}{2}nA\left(\frac{kT_e}{M}\right)^{1/2}, \tag{1}$$

where $I_0$ is the saturation current, $n$ is the ion density, $A$ is the probe surface area, and $M$ is the ion mass. The major limitation of the double-probe technique is that it samples only the high-energy tails of the ion and electron currents, and provides no additional information about the electron energy distribution function (EEDF).

Infrared measurements of the films were made using a Perkin–Elmer 983 spectrophotometer operating in a double-beam optical transmission mode. The hydrogen content of the films was determined through the use of the following equation:

$$N_H=K_H 2.3025\,\frac{\Delta A W}{t}, \tag{2}$$

where $\Delta A$ is the peak absorbance, $W$ is the full peak width at half-maxima, $t$ is the film thickness, $K_H$ is the bond sensitivity factor ($7.1\times10^{16}$ cm$^{-1}$ for SiH, and $8.2\times10^{16}$ cm$^{-1}$ for NH), and $N_H$ is the density of bonds.[5,6,10]

### D. Deposition conditions

The default growth conditions for film deposition are (i) a 300 mTorr pressure, (ii) a total gas flow of 200 sccm through the plasma tube: a mixture of He, and either $N_2$ or $NH_3$, and (iii) a 10 sccm flow of 10% $SiH_4$ in He injected downstream. The applied power is 25 W for the rf plasma, and 170 W for the microwave plasma. In previous studies of thin-film dielectric deposition by the remote PECVD process, we found that deposition rates of the order of

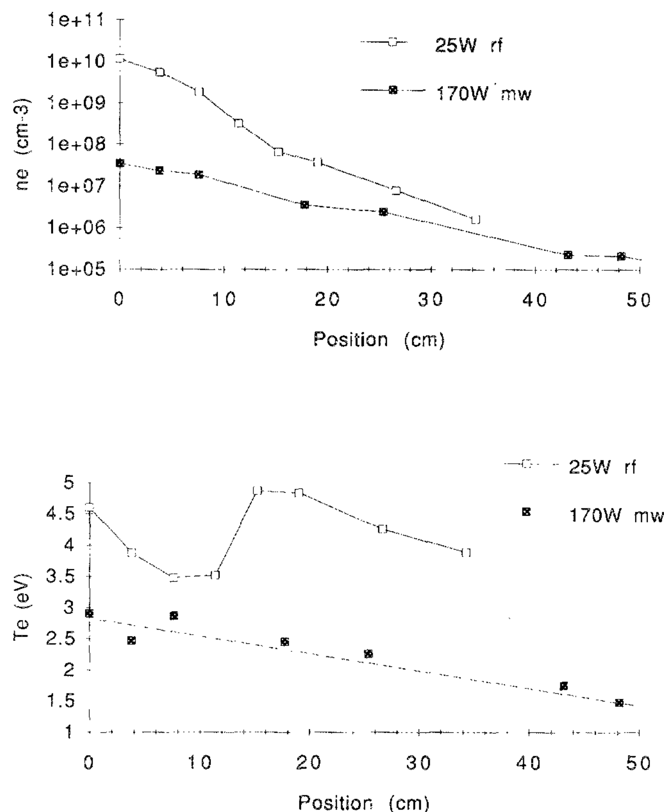


FIG. 2. (a) Charge density $n_e$ as a function of position for rf and microwave plasma excitation of He. (b) Electron temperature $T_e$ as a function of position for rf and microwave deposition. The rf frequency is 13.56 MHz, at 25 W. The microwave frequency is 2.54 GHz at 170 W. The He flow rate is 200 sccm, and the chamber pressure is 300 mTorr. The first dispersal ring is located approximately 10.2 cm from the plasma generation region exit port.

0.1–5 Å/s could readily be obtained for rf plasma power levels of 15–50 W. This led to the choice of 25 W for the rf plasma studies. For the microwave power source and the plasma coupling that we have access to, we were not able to sustain a plasma for power levels below about 150 W, and the 170 W level was chosen to maintain stable microwave discharges. Even though these power level choices are arbitrary, the results we have obtained relative to the nitride deposition mechanisms are indicative of significant qualitative differences between rf and microwave excitation in remote PECVD reactors. All samples were grown at 140 °C so that the films would retain bonded hydrogen in either SiH or Si–NH groups.

## III. RESULTS

### A. Langmuir probe measurements

Figure 2(a) shows the charge density with respect to distance from the exit port of the plasma tube for plasma excitations of 25 W at 13.56 MHz, and 170 W at 2.54 GHz using pure He discharges. The charge density $n_e$ for the 13.56 MHz rf discharge is roughly 2.5 orders of magnitude greater than that of the 2.54 GHz microwave discharge at the plasma tube opening, even though the microwave power level is approximately six times greater. The de-

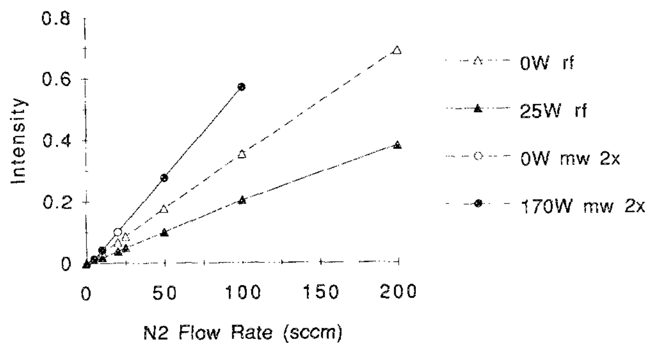


FIG. 3. Mass 14 signal vs $N_2$ flow rate for power off and power on conditions: rf power is 25 W at 13.56 MHz and microwave power is 170 W at 2.54 GHz.

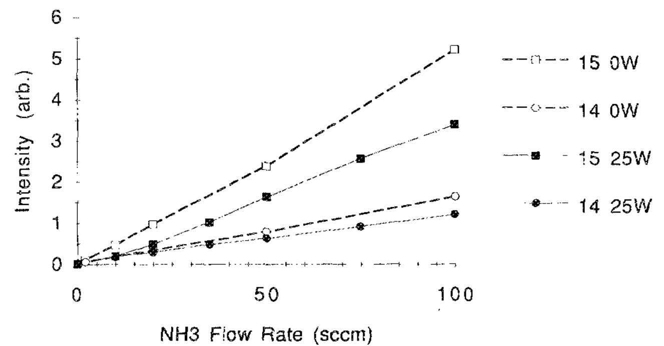


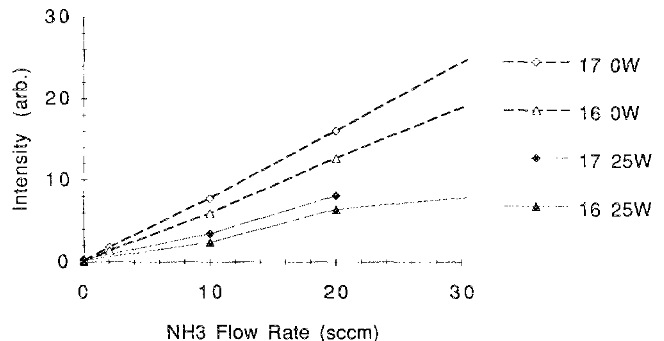


FIG. 4. (a) Mass 14 and mass 15 signals vs $NH_3$ flow rate for power off and for 25 W of rf power at 13.56 MHz. (b) Mass 16 and mass 17 signals vs $NH_3$ flow rate for power off and for 25 W of rf power at 13.56 MHz.

crease in $n_e$ moving away from the plasma tube opening is approximately logarithmic, with the rf density falling off by $\sim$4 orders of magnitude, and the microwave density falling off by $\sim$2.5 orders of magnitude at the far end of the chamber. The electron temperatures $T_e$ are shown in Fig. 2(b) and range from 3.4 to 4.9 eV for the rf discharge, and from 3.0 to 1.5 eV for the microwave discharge. For the rf discharge, and at distances greater than $\sim$18 cm, $T_e$ falls off in the same manner as for the 2.54-GHz discharges, but at distances less than 17 cm, $T_e$ goes through a minimum at $\sim$10 cm, the position of the first dispersal ring which is electrically grounded to the chamber.

### B. Discharge composition

#### 1. $N_2$/He atmosphere

Figure 3 shows the effect of $N_2$ flow rate on the mass 14 signal from the mass spectrometer for the $N_2$/He discharges at 13.56 MHz and 2.54 GHz, with $SiH_4$ injected downstream, and with the mass spectrometer sniffer positioned at the first monitoring station. The four traces show the magnitude of mass 14 for 0 and 25 W at 13.56 MHz, and at 0 and 170 W at 2.54 GHz, with the microwave curves multiplied by a factor of 2. The behavior of each trace is linear with respect to the $N_2$ flow rate. The trace for the 13.56 MHz discharge shows a 40% decrease of mass 14 when $SiH_4$ is injected downstream and the rf power is 25 W; however, no measurable change between the 0 and 25 W rf excitations was detected when the $SiH_4$ flow was reduced to zero. For the 2.54 GHz discharges the change in mass 14 for the power levels of 0 and 170 W is within the noise limit for detection, $\sim$1%. The mass 14 signals for the rf and microwave discharges are attributed to $N_2$. In particular there were no precursors formed with Si–N bonds, as for example aminosilanes or siloxanes. In addition (i) there were no polysilane, $Si_xH_y$ mass features detected under any conditions examined, and (ii) there were no significant changes in the hydrogen signals under any of the experimental conditions explored, including whether or not $SiH_4$ was flowing.

#### 2. $NH_3$/He atmosphere

Figures 4(a) and 4(b) shows the mass spectrometer signals for masses 14 and 15, and masses 16 and 17, respectively, as a function of the $NH_3$ flow rate for 13.56 MHz discharges with the $SiH_4$ flow on. Mass 14 corresponds to N, mass 15 to NH, mass 16 to $NH_2$, and mass 17 to $NH_3$. Wherever appropriate, corrections were made to the data by subtracting away background levels for gases such as O, mass 16, and OH, mass 17, etc. Figures 4(a) and 4(b) shows measurable decreases in the corrected signals for masses, 14–17, when the rf power is increased from 0 to 25 W. The fractional decreases are less for masses 14

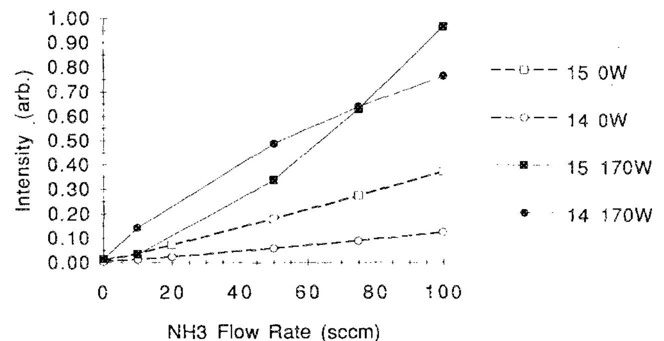


FIG. 5. Mass 14 and mass 15 signals vs $NH_3$ flow rate for power off and for 170 W of microwave power at 2.54 GHz.

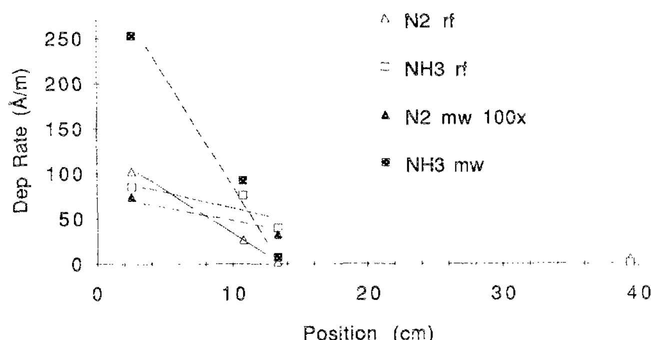


FIG. 6. Deposition rate vs position relative to the plasma excitation tube exit port for $N_2$/He and $NH_3$/He mixtures excited with 25 W or rf at 13.56 MHz and 170 W of microwave power at 2.54 GHz. The total flow rate is 200 sccm, and the relative flow rates of $N_2$ and $NH_3$ are 50 sccm.

and 15 than for masses 16 and 17. Mass 14 shows a 20% change relative to ~35% changes for masses 16 and 17, while mass 15 shows a slightly increased change of 25%.

For the 2.54 GHz discharges, the traces in Fig. 5 for masses 14 and 15 display increases when the microwave power is increased from 0 to 170 W. Mass 15 increases superlinearly $NH_3$ flow; however, the mass 14 trace shows a saturation at flow rates of $NH_3$ above about 30 sccm. Additional comparisons of the changes in mass 14 with $NH_3$ flow, to changes in masses 28, $N_2$, and 17, $NH_3$, show that mass 14 derives almost entirely from these species, with at most 5% coming from other species entering the sniffer port. It should be noted that 3–4 times more hydrogen is produced in the 2.54 GHz discharges than in the 13.56 MHz discharges, and that the film deposition rate, as shown in Fig. 6 tracks the production of H.

### C. Nitride deposition

The deposition rate and hydrogen content with respect to position from the end of the plasma tube are shown, respectively, in Figs. 6 and 7, for both the $N_2$/He and $NH_3$/He discharges. The plasma power is 25 W at 13.56 MHz, and 170 W at 2.54 GHz, and the flow rates are 10 sccm 10% $SiH_4$ in He, downstream, and 150 sccm He, with either 50 sccm of $N_2$ or $NH_3$ injected through the plasma-excitation tube. All of the deposition rates decrease with increasing distance from the plasma generation region, but at different rates. The highest growth deposition rates occur closest to the plasma tube, and all deposition rates reach negligible rates 40 cm downstream from the plasma generation region. With rf excitation, the deposition rates are comparable for the two N-atom sources gases at the 5 cm position, but deposition from the $N_2$ source gas drops more rapidly than deposition from the $NH_3$ source gas. In particular, there is no detectable deposition beyond the 14 cm point with the $N_2$ source gas, whereas the deposition rate using the $NH_3$ source gas has only fallen by about 50% at the same point. The deposition rates using the 2.54 GHz microwave excitation are very different from those using rf excitation. The 2.54 GHz $NH_3$/He discharge produces a deposition rate that is 2 times *higher* than the deposition rate with the 13.56 MHz discharge at the 3 cm position, while the microwave excitation of the $N_2$/He mixture generates a deposition rate that is 140 times *lower* compared with $N_2$/He excitation by the 13.56 MHz rf discharge. In addition, we have observed that hydrogenated amorphous silicon, *a*-Si:H, films can be grown using rf discharges of He alone, but cannot be grown using microwave discharges of He alone. Deposition of a film using the 2.54 GHz microwave source requires simultaneous excitation of He and either $N_2$ or $NH_3$, with film growth being much more effective, by factors of several hundred, with $NH_3$ source gas mixtures. Films of *a*-Si:H and microcrystalline silicon, $\mu c$-Si have been grown by 2.54 GHz excitation of $H_2$.[11,12]

Figure 7 shows the bonded hydrogen concentrations as SiH and Si–NH for the films produced using the 13.56 MHz rf discharge films. The concentrations were determined from the analysis of ir absorption data in the bond-stretching frequency regimes of 2000–2200 $cm^{-1}$ for SiH, and 3000–3500 $cm^{-1}$ for Si–NH. For depositions near the plasma tube opening at the 2.5 cm position, the total bonded H concentrations are within about a factor of 2 for films grown by excitation using the $N_2$/He and $NH_3$/He source gas mixtures, $2.3\times10^{22}$ $cm^{-3}$ for the $N_2$ mixture, and $4.0\times10^{22}$ $cm^{-3}$ for the $NH_3$ mixture. However the H atoms are predominantly in Si–H bonds using the $N_2$ N-atom source gas, and predominantly in Si–NH bonds using the $NH_3$ source gas. Moreover, there is virtually no detectable SiH in the films deposited from the $NH_3$ source gas mixture, while there are at best trace amounts of Si–NH in the films grown from the $N_2$ source case mixture. For all of the deposition positions, the films deposited using the $NH_3$ source gas contain more bonded hydrogen than films deposited using the $N_2$ source gas. The hydrogen concentration decreases with deposition rate in both processes.

We could not detect bonded H in the films produced by microwave excitation of $N_2$/He source gases, simply because the films were too thin. The bonded hydrogen for films grown by microwave excitation of $NH_3$/He mixtures showed both SiH and Si–NH bonding. For the 50 sccm flow rate of $NH_3$, the [Si–NH]/[SiH] ratio is about 3 for plasma excitation using the 2.54 GHz microwave dis-

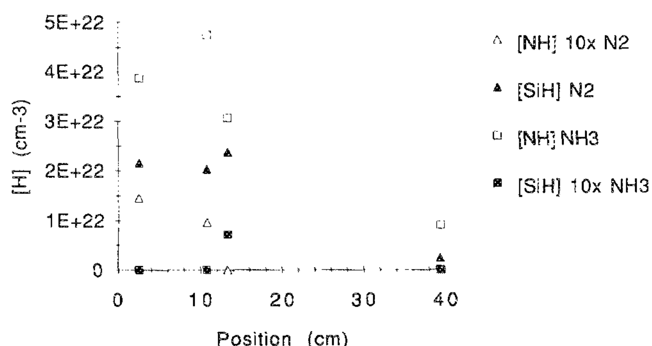


FIG. 7. Bonded hydrogen in SiH and Si–NH groups a function of position relative to the exit port from the plasma generation tube. The first dispersal ring is located approximately 10.2 cm from the plasma generation region exit port.

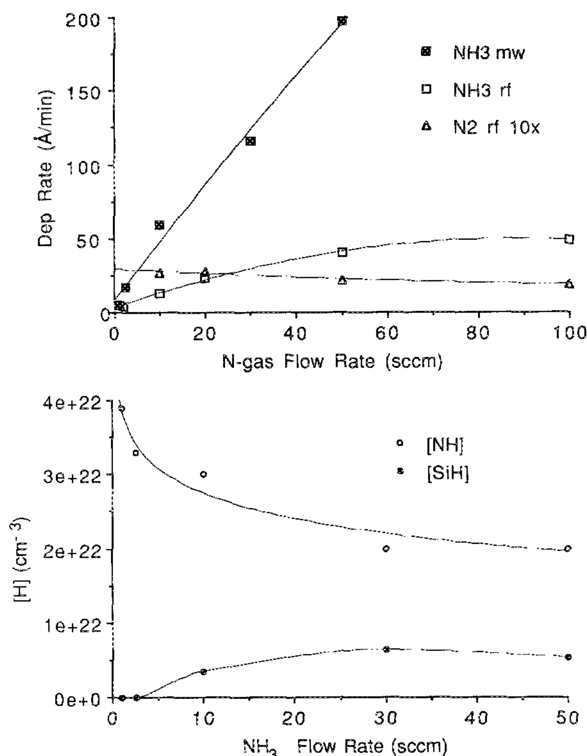


FIG. 8. (a) Deposition rate as a function of the nitrogen-atom source gas flow for $N_2$ and $NH_3$, excited by rf, and $NH_3$ excited by microwaves. (b) Bonded hydrogen content as a function of $NH_3$ gas flow rate. The total nitrogen-atom source gas plus He flow was 200 sccm.

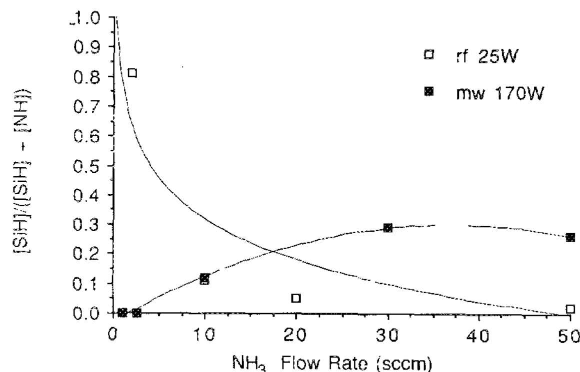


FIG. 9. This figure shows the fraction of silicon-bonded H in SiH bonded groups relative to the total bonded hydrogen concentration in both SiH and Si–NH groups a function of the $NH_3$ gas flow rate for the two excitation frequencies: 13.56 MHz and 2.54 GHz.

charge, whereas this same ratio is more than 100 using the same gas flows and 13.56 MHz rf excitation.

Figure 8(a) shows the deposition rate as a function of both N-atom source gas flow rates at the 13 cm downstream growth position for 13.56 MHz excitation, and for the $NH_3$ flow rate for 2.54 GHz excitation for the 2.5 cm downstream growth position. Using rf excitation and the $N_2$/He source gas mixture, the deposition rate changes very little from an average rate of about 2 Å/min over the entire range of $N_2$ flow rates studied for 10–100 sccm. Note that the total $N_2$ + He flow rate was held at 200 sccm. The same constraint on total flow rate holds for the $NH_3$ + He mixtures. The $NH_3$ process using rf excitation shows a linear increase in deposition with $NH_3$ flow rate growth rate up to about 30 sccm, and shows saturation tending to growth rate of $\sim$50 Å/min for flow rates between about 30 and 100 sccm. The deposition rate for the microwave excitation was measured at a position closer to the plasma tube and shows considerably higher deposition rates. The deposition is essentially linear with the $NH_3$ flow rate for flow rates up to about 50 sccm, with a value of about 200 Å/min at the 50 sccm flow rate. Note that the deposition rate for microwave excitation of $NH_3$ at the 14 cm position was essentially zero for an $NH_3$ flow rate of 50 sccm.

Figure 8(b) shows the bonded hydrogen concentrations as Si–NH and SiH as a function of the $NH_3$ flow rate for 2.54 GHz microwave excitation. At the lowest flow rates of 1–2 sccm, the bonded hydrogen is present almost entirely as Si–NH. As the flow is increased the Si–NH concentration drops off in a nonlinear manner, falling faster than linearly between about 1–2 sccm and 30 sccm, and then tending toward flow rate independent concentration between 30 and 50 sccm. The bonded H concentration in SiH groups is essentially zero for $NH_3$ flow rates of 1–2 sccm, and then rises up to about 30 sccm, and saturates for flow rates between about 30 and 50 sccm of $NH_3$ flow. For flow rates between 30 and 50 sccm, the ratio of Si–NH to SiH bonds is about three to one. This behavior is different from the bonded hydrogen in films grown from similar $NH_3$/He mixtures, but with rf excitation at 13.56 MHz. For these films, very dilute $NH_3$ mixtures, $<1\%$ $NH_3$ flow to He flow, resulted in films where the dominant bonded hydrogen was in SiH groups, whereas higher concentrations flow rate ratios of $NH_3$ to He also resulted in Si–NH groups being the dominant H-atom bonding configuration. For 13.56 MHz rf excitation of $N_2$/He mixtures, the incorporation of hydrogen is dominated by SiH bonding groups at all flow rate ratios, with no ir detectable Si–NH groups in the films.

Finally, Fig. 9 shows the fraction of silicon-bonded H in SiH bonded groups relative to the total bonded hydrogen concentration in both SiH and Si–NH groups a function of the $NH_3$ gas flow rate for the two excitation frequencies. For 13.56 MHz rf excitation, the fraction of SiH bonding drops by a factor of more than 16 from 80% to about 5%, as the $NH_3$ flow rate increases from about 2.5 to 20 sccm. As the flow rate of $NH_3$ is increased to 50 sccm, the fraction of SiH bonding continues to fall with increasing $NH_3$ flow, but at a much reduced rate. In contrast the fraction of SiH groups in the films produced by 2.54 GHz microwave excitation increased with increasing $NH_3$ flow, approaching a fraction of approximately 30% for $NH_3$ flow rates between 30 and 50 sccm.

## IV. DISCUSSION

### A. Plasma coupling mechanisms

The lower charge density for the 2.54 GHz microwave discharge as compared to the 13.56 MHz rf discharge, as shown in Fig. 2, is consistent with previously reported

work, and is explained by the differences in coupling between the plasma and the chamber for these two plasma excitation frequencies.[13,14] It has been established, that for an electrodeless discharge created in a glass envelope, the charge density is significantly higher for microwave than for rf discharges.[15–17] This difference in charge density in the excitation region is not maintained in the *chamber* used for this study because of differences in the way the electric field of the plasma discharge extends beyond the plasma excitation region. This difference in plasma containment is a direct result of the different electrode configurations used for initiating and maintaining the two types of plasma discharges. The observation that $T_e$ *increases* between 13 and 17 cm for 13.56 MHz discharges, demonstrates that electrons are being accelerated in the chamber, indicating that a significant electric field is present near grounded chamber surfaces, in this case the first gas dispersal ring. This acceleration is a manifestation of the fact that the rf power is capacitively coupled into the plasma.[18,19] This mode of coupling is consistent with the following observations: (i) the end of the coil that wraps around the plasma tube is not electrically connected to ground, yet, it is still possible to ignite and sustain the plasma; (ii) if the plasma is ignited and if the end of the coil is then grounded, the plasma is extinguished, and (iii) the ac impedance for coupling of the rf power to the plasma is a net capacitive impedance. Under these excitation conditions, the electric field between the powered electrode and the grounded chamber accelerates negative charge, predominantly electrons, out of the plasma tube and into the chamber. This had been previously demonstrated in studies of the deposition mechanisms for silicon dioxide $SiO_2$, and silicon suboxide $SiO_x$ with $x<2$, films.[18,19] Figure 2(b) shows that the 2.54 GHz discharge does not show the same degree of negative charge transport into the chamber, demonstrating that any electric fields extending into the chamber are significantly reduced, even though the power level used was significantly higher than in the rf case. For the microwave discharge, negative charge can only be transported into the chamber by either thermal diffusion, and gas flow. We therefore conclude that electrons are more likely to play a role in deposition reactions for the 13.56 MHz rf excitation than for the 2.45 GHz microwave excitation, simply because of the electrode structures used to ignite and sustain the plasmas in these two different frequency regimes.

## B. Deposition mechanisms

### 1. Deposition from He discharges

Previous experiments have shown that *a*-Si:H films can be deposited by extracting active species from rf-excited He discharges in chambers similar to the one used in these studies.[18,19] The deposition process utilizes heterogeneous reactions that take place at the deposition substrate. whereas precursor activation and/or formation can either occur in the gas phase or at the substrate. These experiments have also demonstrated that the deposition process reactions are driven by negatively charged species, predominantly electrons, that are transported from the plasma excitation region into the deposition region of the chamber.[18,19] We have observed that *a*-Si:H films can be deposited from He discharges using rf excitation, but that *a*-Si:H films cannot be deposited using microwave discharges of He. Based on the results displayed in Fig. 2, these results are consistent with the deposition reaction pathways identified in the previously reported studies.[18,19] The density of charge particles, i.e., electrons, transported out the plasma excitation region of the rf plasma due to the electrode geometry is sufficiently high to promote a heterogeneous CVD interaction at the deposition substrate, while the density of electrons extracted from the microwave plasma is insufficient to promote measurable film deposition.

### 2. Deposition for $N_2$/He discharges

Our studies have shown that *a*-Si:H films cannot be deposited using $N_2$/He mixtures under any microwave plasma excitation conditions explored. However, using $N_2$/He mixtures nitride films can be deposited with microwave excitation, but only with very low deposition rates. This means that active N species, e.g., N atoms or ions, transported out of the plasma excitation region into the deposition region can promote measurable film deposition, but that He metastables or electrons are not created in sufficient numbers to promote any parallel film deposition reactions. In contrast, silicon nitride films have been deposited using rf excitation of $N_2$/He source gas mixtures. Ir studies have shown that these films can contain bonded hydrogen in both SiH and Si–NH configurations (see Fig. 7). Films deposited between the first dispersal ring, where the $SiH_4$ is injected, and the plasma tube have both types of bonded hydrogen arrangements, whereas films deposited downstream from the first dispersal ring have predominantly SiH groups and are subnitrides. $SiN_x$, with $x<1.33$, as well. We interpret these results as follows: (i) film deposition beyond the first dispersal ring is driven primarily by energetic electrons that are transported into the chamber under the influence of the electric field associated with the plasma excitation electrode geometry, i.e., where the first dispersal ring acts a ground for accelerating electrons downstream [see Figs. 2(a) and 2(b)]. In the region between the dispersal ring and the plasma tube, $SiH_4$ injected downstream can diffuse back into the mouth of the excitation tube and be fragmented in high-energy electrons. This process produces atomic hydrogen which drives a deposition reaction which incorporates H atoms in both SiH and Si–NH bonding configurations. This type of mechanism is supported by our studies of deposition from $NH_3$/He plasmas, and by the previously reported studies of Johnson *et al.*[11,12] The results reported above are again consistent with precursor formation and/activation occurring either in the gas phase or at the deposition substrate, but with the deposition reactions taking place at the film surface. This means that species with Si–N bonding arrangements are not formed in the gas phase, but are generated at the film surface through heterogeneous chemical reactions.

### 3. Deposition for $NH_3$/He discharges

The data in Fig. 9 shows the distribution of bonded hydrogen between SiH and Si–NH groups is different for films deposited by rf and microwave excitation of $NH_3$/He source gas mixtures demonstrating that the deposition reaction pathways using rf and microwave excitation are different. These studies also imply that there are different chemically driven $SiH_4$ and $NH_3$ break-up reactions that contribute to the two film growth processes. For both rf and microwave excitation the deposition rate increases with increasing $NH_3$ flow rate for source gas mixtures that contain at least up to 50 sccm of $NH_3$, or up to 25% of total $NH_3$/He flow of 200 sccm. However, the chemical composition of the films with respect to incorporation of bonded H is qualitatively different as shown in Figs. 7–9. For example, films grown at very low $NH_3$ flow rates are dominated by SiH bonding, whereas films deposited at higher $NH_3$ flow rates are dominated by Si–NH bonding. We interpret this in the following way: (i) film deposition for low $NH_3$ flow rates involves two Si-atom and N-atoms source gas activation mechanisms driven respectively by (a) the creation of H and NH groups in the plasma, and (b) the break-up of $SiH_4$ by energetic electrons extracted from the plasma; and (ii) film deposition at higher $NH_3$ flow rates involves predominantly deposition reactions driven by the H and NH groups generated within the plasma region. This proposed mechanism for film growth reactions is consistent with the previously reported studies of suboxide deposition, in which two parallel mechanisms dominated in the suboxide deposition region: (a) deposition of an *a*-Si:H alloy component with SiH bonds that derived from electrons exciting the $SiH_4$ reactant, and (b) deposition of an $SiO_2$ component that derived from active O species reacting heterogeneously at the substrate with the $SiH_4$.[18,19] Suboxides could be deposited at low $O_2$ flow rates where He metastable production was not quenched. The He metastable production was correlated with the generation of significant numbers of energetic electrons ($E \sim 5$–10 eV) via Penning-type processes. At higher flow rates, He metastable production was reduced, and deposition reactions were driven by O species, predominantly long-lived $O_2$ metastables.[16,17,20] Spectroscopic studies of He metastable formation, and quenching in $NH_3$/He plasmas as a function of the $NH_3$ concentration give further support to this proposed mechanism.[20]

The distribution of bonded H between SiH and Si–NH in the nitride films deposited using microwave excitation of $NH_3$/He source gas mixtures is qualitatively different as displayed in Figs. 7–9. Films deposited at the lowest $NH_3$ flow rates can be driven by H and NH species extracted from the plasma. However, the absence of SiH groups in these films suggests that these species react with the $SiH_4$ at the substrate and produce nitride films with Si–NH groups, the same mechanism as in the high flow rate regime for rf excitation of $NH_3$/He mixtures. Comparisons with the microwave deposition of *a*-Si:H by Johnson *et al.*[11,12] then suggest that at these low flow rates excitation by NH groups and not H, dominates. At the higher flow rates, the simultaneous occurrence of significant concentrations of both SiH and Si–NH groups suggest two parallel deposition reactions: (a) one pathway leading to a hydrogenated nitride alloy component with Si–NH bonding and driven by plasma generated NH, and (b) a second pathway leading to the formation of an *a*-Si:H component with SiH bonding and driven by plasma generated atomic H. These pathways are consistent with the experimental results, and the deposition reactions models as reported by Johnson *et al.*[11,12] The proposed pathways are also consistent with model calculations of reaction pathways. For example, Kushner has demonstrated that $H + SiH_x \rightarrow H_2 + SiH_{x-1}$, and these types of reactions lead to significant radical formation,[21] in particular to the generation of $SiH_2$ and $SiH_3$ radicals, both of which can promote deposition of an *a*-Si:H alloy component. Again, it should be noted that Si–N bonding arrangements are formed via heterogeneous reactions at the deposition substrate, but that precursor formation and/or activation can occur either in the gas phase or at the deposition substrate, again subject to the constraint that precursor species with Si–N bonds are formed only at the deposition substrate.

## V. SUMMARY

The results of our studies have demonstrated that there are two different reaction pathways for film deposition of nitrides from plasma excited $N_2$/He and $NH_3$/He source gas mixtures. Deposition of nitride films from $N_2$/He source gases mixtures was achieved with rf excitation, but not with microwave excitation. The differences in bonded hydrogen for substrate placement is consistent with two reaction pathways: (a) one pathway for an *a*-Si,N:H alloy component that is driven by electron excitation and N-atom production that occurs at all substrate positions; and (b) a second driven by direct excitation and breakup of the $SiH_4$.

Nitride films are obtained for both rf and microwave excitation of $NH_3$/He mixtures, and our studies indicate that deposition reactions in this case are driven primarily by H atoms, and to a lesser extend by electrons. This is true even though high densities of electrons are produced within the microwave discharge region. Two different deposition pathways have been identified by varying the relative flow rate of $NH_3$ to He. For the rf discharges, high concentrations of SiH bonds, that are found for low $NH_3$ to He ratios are consistent with electron driven reactions involving the breakup of the $SiH_4$ reactant, whereas, for high $NH_3$ to He ratios low SiH concentrations, but significant concentrations of Si–NH are consistent with deposition reactions driven by plasma generated fragments of the $NH_3$ molecule. Microwave excitation of $NH_3$/He mixtures yields different results, with low concentrations of $NH_3$ to He yielding films are dominated by Si–NH bonding, and higher concentrations of $NH_3$ to He yielding films that display significant concentrations of both SiH and Si–NH bonding groups. For low concentrations of $NH_3$ to He, the depositions are driven by plasma generated N and NH species, whereas for the higher concentrations of $NH_3$ to He, the reactions are driven by H atoms which open up a

pathway in which the $SiH_4$ molecule is fragmented, leading to significant SiH incorporation.

The method of coupling microwave power into the plasma does not generate electric fields that extend out of the plasma generation region and into the chamber, so that the electron densities available for excitation in the chamber region are significantly reduced with respect to the rf excitation studies where the excitation geometry we employed promotes significant field penetrations into the deposition region of the chamber.

## ACKNOWLEDGMENTS

This work is supported by ONR, the NSF Engineering Research Center at NC State University for Advanced Electronic Materials Processing, and the NC State University Sematech Center of Excellence.

[1]D. L. Smith, Mater. Res. Soc. Symp. Proc. **165**, 69 (1990).
[2]P. Boher, M. Renaud, L. J. Van Ijzendoorn, J. Barrier, and Y. Hily, J. Appl. Phys. **63**, 1464 (1988).
[3]E. C. Paloura, J. Lagowski, and H. C. Gatos, J. Appl. Phys. **69**, 3995 (1991).
[4]S. V. Hattangady, G. G. Fountain, R. A. Rudder, and R. J. Markunas, J. Vac. Sci. Technol. A 7, 570 (1989).
[5]D. V. Tsu, G. Lucovsky, and M. Mantini, Phys. Rev. B **33**, 7069 (1985).
[6]D. V. Tsu and G. Lucovsky, J. Vac. Sci. Technol. A **4**, 480 (1986).
[7]D. V. Tsu, G. Lucovsky, M. Mantini, and S. S. Chao, J. Vac. Sci. Technol. A **5**, 1998 (1987).
[8]E. O. Johnson and L. Malter, Phys. Rev. **80**, 58 (1950).
[9]*Plasma Diagnostics*, edited by R. H. Huddlestone and S. L. Leonard (Academic, New York, 1965), pp. 113–200.
[10]A. C. Adams, Solid State Technol. **26**, 135 (1983).
[11]N. M. Johnson, S. E. Ready, J. B. Boyce, C. D. Doland, S. H. Wolf, and J. Walker, Appl. Phys. Lett. **53**, 1626 (1988).
[12]N. M. Johnson, J. Walker, C. M. Doland, K. Winer, and R. A. Street, Appl. Phys. Lett. **54**, 1872 (1989).
[13]D. Landheer *et al.*, J. Vac. Sci. Technol. A **9**, 2594 (1991).
[14]B. Anthony, T. Hsu, R. Qian, J. Irby, S. Banerjee, and A. Tasch, J. Electron. Mater. **20**, 309 (1991).
[15]C. M. Ferreira and J. Loureiro, J. Phys. D **17**, 1175 (1984).
[16]M. R. Wertheimer and M. Moisan, J. Vac. Sci. Technol. A **3**, 2643 (1985).
[17]M. Moisan, C. Barbeau, R. Claude, C. M. Ferreira, J. Margot, J. Paraszczak, A. B. Sá, G. Sauvé, and M. R. Wertheimer, J. Vac. Sci. Technol. A **9**, 8 (1991).
[18]D. V. Tsu, G. N. Parsons, and G. Lucovsky, J. Vac. Sci. Technol. A **6**, 1849 (1988).
[19]D. V. Tsu, G. N. Parsons, G. Lucovsky, and M. W. Watkins, J. Vac. Sci. Technol. A **7**, 1115 (1989).
[20]G. Lucovsky, D. V. Tsu, R. A. Rudder, and R. J. Markunas, in *Thin Film Processes II*, edited by J. L. Vossen and W. Kern (Academic, New York, 1991), p. 565, and references therein.
[21]M. J. Kushner, J. Appl. Phys. **63**, 2532 (1988).